SPECIAL ISSUE ARTICLE

European Journal of **Soil Science** **WILEY**

A field system for measuring plant and soil carbon fluxes using stable isotope methods

Christopher S. McCloskey[1,2] | **Wilfred Otten[1]** | **Eric Paterson[2]** |
Ben Ingram[1] | **Guy J. D. Kirk[1]**

[1]School of Water, Energy & Environment, Cranfield University, Bedford, UK

[2]The James Hutton Institute, Aberdeen, Scotland

Correspondence
Chris McCloskey, School of Water, Energy & Environment, Cranfield University, Cranfield, Bedford MK43 0AL, UK.
Email: c.mccloskey@cranfield.ac.uk

Abstract

There is a lack of field methods for measuring plant and soil processes controlling soil organic matter (SOM) turnover over diurnal, seasonal and longer timescales with which to develop datasets for modelling. We describe an automated field system for measuring plant and soil carbon fluxes over such timescales using stable isotope methods, and we assess its performance. The system comprises 24 large (1-m deep, 0.8-m diameter) cylindrical lysimeters connected to gas-flux chambers and instruments. The lysimeters contain intact, naturally structured C3 soil planted with a C4 grass. Fluxes of CO_2 and their ^{13}C isotope composition are measured three times daily in each lysimeter, and the isotope composition is used to partition the fluxes between plant and soil sources. We investigate the following potential sources of error in the measurement system and show they do not significantly affect the measured CO_2 fluxes or isotope signatures: gas leaks, the rate of gas flow through sampling loops, instrument precision and drift, the concentration dependence of isotope measurements, and the linearity of CO_2 accumulation in the chambers and associated isotope fractionation resulting from different rates of $^{13}CO_2$ and $^{12}CO_2$ diffusion from the soil. For the loamy grassland soil and US prairie grass (*Bouteloua dactyloides*) tested, the precision of CO_2 flux measurements was ±0.04% and that of the flux partitioning ±0.40%. We give examples of diurnal and seasonal patterns of plant and soil C fluxes and soil temperature and moisture. We discuss the limitations of the isotope methodology for partitioning fluxes as applied in our system. We conclude that the system is suitable for measuring net ecosystem respiration fluxes and their plant and soil components with sufficient precision to resolve diurnal and seasonal patterns.

Highlights

- We describe an automated system for measuring plant and soil carbon fluxes under field conditions.
- We exploit the large difference in isotope signatures between C3 and C4 soils and plants to partition the net flux.
- Possible sources of error are quantified and shown to be small.
- The system is capable of resolving diurnal and seasonal patterns.

1 | INTRODUCTION

Measurements of soil-atmosphere carbon (C) fluxes necessarily conflate fluxes from plants and recent plant inputs with those from the decomposition of existing soil organic matter (SOM). It is essential to disentangle the two to measure the true response of SOM turnover to driving variables. How to do this under field conditions is a key problem in studies of ecosystem C balances. In this paper we describe an automated field system for measuring plant and soil C fluxes separately using stable isotope methods, and we assess the limitations of the isotope methodology for partitioning fluxes as applied in our system.

Bowling, Pataki, and Randerson (2008), Paterson, Midwood, and Millard (2009) and Zhu, Di, Ma, and Shi (2019) review stable isotope approaches to quantify plant and soil C fluxes. The natural isotope composition of CO_2 (as gauged by $\delta^{13}C$) derived from SOM turnover differs from that from plant C turnover by small but detectable amounts. In principle, this provides a means of separating the plant and SOM-derived fluxes. However, this approach requires a high degree of analytical precision, and isotopic partitioning may be confounded by minor variations in isotopic discrimination, such as during plant water stress. A much larger difference in $\delta^{13}C$ between plant and soil sources can be created by growing the plants in an atmosphere with CO_2 depleted or enriched in ^{13}C so as to continuously label the plant C inputs to the soil. Such continuous labelling has the advantages over "pulse" labelling in that plant-derived C is homogenously labelled, allowing quantitative partitioning of the CO_2 efflux. Continuous ^{13}C-labelling has been used in laboratory experiments to partition plant and soil sources, and to follow incorporation of plant-derived C into soil pools (Garcia-Pausas & Paterson, 2011; Schnyder, Schäufele, Lötscher, & Gebbing, 2003). The potential for this under field conditions has been demonstrated in free-air CO_2 enrichment (FACE) experiments where long-term fumigation with fossil-derived CO_2 has inadvertently provided a ^{13}C-label for plant inputs relative to soil (Carney, Hungate, Drake, & Megonigal, 2007; Iversen, Keller, Garten Jr, & Norby, 2012; Taneva, Pippen, Schlesinger, & Gonzàlez-Maler, 2006). However, this requires costly apparatus and large quantities of CO_2.

An alternative, more practicable approach is to exploit differences in the isotope signatures of plants with C3 versus C4 photosynthetic pathways (Farquhar, Ehleringer, & Hubick, 1989). Plants with C4 photosynthesis typically respire CO_2 with $\delta^{13}C$ of approximately −12‰ (range −9 to −19‰), whereas those with C3 photosynthesis typically have approximately −27‰ (range −23 to −40‰) (Balesdent, Mariotti, & Guillet, 1987). This provides a difference in $\delta^{13}C$ an order of magnitude larger than that between C3 plants and C3 SOM. Most studies exploiting these differences have been laboratory based and therefore not representative of undisturbed field soils, nor of in-field seasonal and annual climatic variations. Further, such studies are usually short term, lasting only a few weeks or months. In longer-term studies (e.g., Bader & Cheng, 2007; Dijkstra & Cheng, 2007; Lu, Dijkstra, Wang, & Cheng, 2009), measurements are generally infrequent. To date only a few studies have exploited plant and soil $\delta^{13}C$ differences to measure SOM turnover under field conditions (Millard, Midwood, Hunt, Whitehead, & Boutton, 2008; Moinet et al., 2018; Snell, Robinson, & Midwood, 2014). These have relied on manual sample collection and processing, limiting the practicality of collecting long-term continuous datasets. Methods have been developed using portable chambers deployed in the field (e.g., Snell et al., 2014), but so far only for periods of a few weeks.

We have developed a field system allowing near-continuous, long-term measurements of soil and plant C fluxes and their drivers over multiple growing seasons, with C4 plants in C3 soils. We describe the system here and assess potential sources of error and the overall precision of the system. We assess how well plant and soil fluxes are separated, and how well diurnal and seasonal patterns in plant and soil fluxes can be quantified.
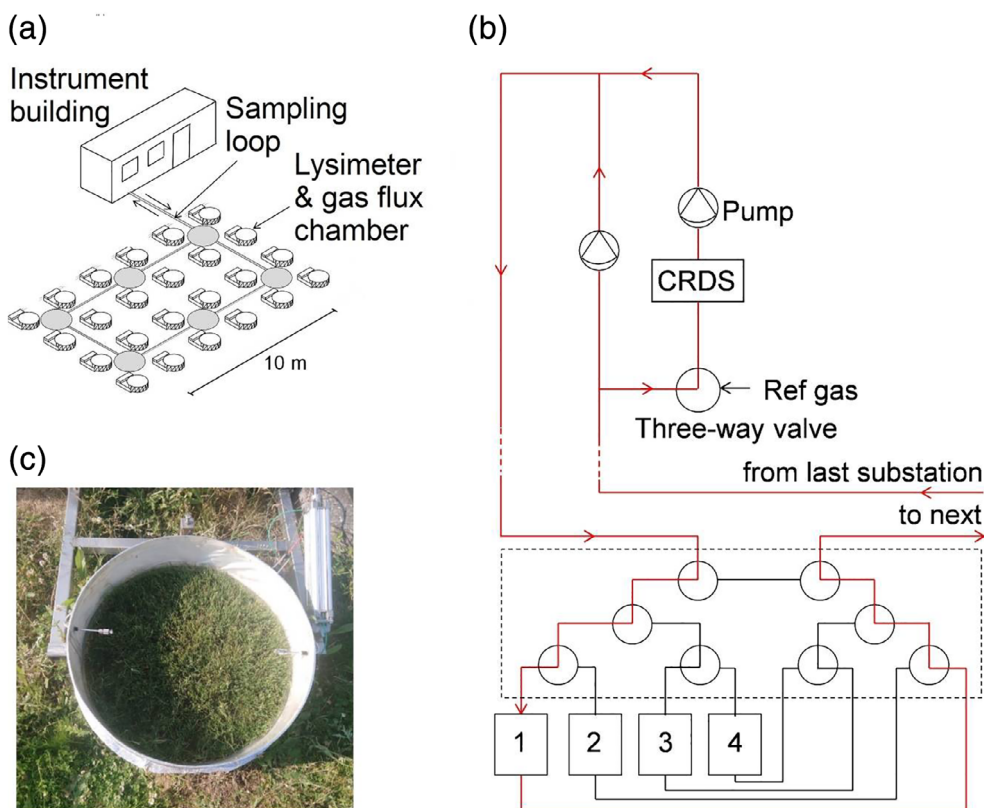
FIGURE 1 The field laboratory. (a) Layout of the 24 lysimeters around six manifold substations. (b) Schematic of a manifold substation (inside dashed line) connecting four lysimeters (numbered boxes) to the main sampling loop and a subsampling loop containing a cavity ring-down spectroscopy (CRDS) isotope analyser and reference gas unit. The valves are set for flow through chamber 1 (red lines). (c) Vertical view of a lysimeter and its gas flux chamber with C4 buffalo grass growing in a C3 soil monolith

2 | MATERIALS AND METHODS

2.1 | System overview

The system comprises 24 cylindrical hydrologically isolated, 1-m deep, 0.8-m diameter lysimeters containing intact soil monoliths and connected to gas-flux chambers with pneumatically operated lids (Figure 1). Gases accumulating when the lids are closed are circulated through a closed loop to gas analysis instruments in an instrument building. The closing of the chamber lids and the directing of gas flow to and from the chambers are controlled by bespoke software.

The soil monoliths were obtained intact (i.e., without changing inherent soil structure) from field sites and brought to Cranfield in southeast England. They are contained in glass-fibre sleeves with 5-mm thick walls and galvanized iron trays at the base to collect leachate. They were collected by driving the glass-fibre sleeves into the ground whilst digging the surrounding soil away and making a trench to one side, and then cutting the monolith at the base by driving across a steel plate with a car jack. There are two soil types: (a) a well-drained coarse loamy soil formerly under bracken/grass at Shuttleworth College, Bedfordshire, with initial properties (0–15 cm) pH 5.0 and organic C 62 g·kg^{-1}, and (b) a poorly drained, seasonally waterlogged loamy soil over clay formerly

under old pasture at Temple Balsall, Warwickshire, with properties pH 5.4 and organic C 43 g·kg^{-1}. Only results for the Temple Balsall soil are given here. The soil monoliths are buried so that the soil surface is flush with the surroundings. Temperature and moisture at depths of 6 and 12 cm are measured with Delta-T SM150T sensors (5-min resolution). Water and dissolved solutes passing out of the bottom are collected. The site has a weather station (Vaisala WXT520), which measures wind speed and direction, precipitation, barometric pressure, temperature and relative humidity.

In January 2018, the lysimeters were sown with a single C4 pasture-grass species, *Bouteloua dactyloides* (buffalo grass), native to the North American prairies (USDA, 2019). This was shown to be suited to the two soils in a preliminary pot trial in which we grew it with three other C4 species from similar habitats (*Bouteloua curtipendula*, sideoats grama; *Bouteloua gracilis*, blue grama; and *Schizachyrium scoparium*, little bluestem), and found *B. dactyloides* established most successfully and had the greatest growth rate. It has been maintained in the lysimeters at a mean canopy height of 10 cm by periodic clipping, reaching 20 cm height between clippings. The soils contain C3 organic matter, having only ever previously been exposed to C3 vegetation. The C isotope signature of CO_2 emitted from the soil can therefore be used to partition the CO_2 flux between plant and soil sources (Section 2.2.3).

2.2 | Gas sampling and analysis

2.2.1 | Lysimeter chambers and main sampling loop

The lysimeters are arranged in six groups of four around six manholes to which they are connected at different depths (Figure 1a). The manholes contain manifolds to deliver gases to analytical instruments, collectors for the lysimeter drainage, and connections for the chamber pneumatics and soil temperature and moisture sensors.

Each chamber has a pneumatically operated 80-cm diameter lid, which closes to give a gas-tight seal. The lid contains a 5-cm diameter vent valve, which closes a few seconds after the lid to dampen pressure changes. The chamber wall and lid are made of 10-mm-thick clear acrylic plastic. The wall and lid are covered in reflective foil-backed glass-fibre cloth and the lid cover is removable to allow flux measurements to be made in both dark and light conditions. The height of the lid above the soil surface is 26 cm, so the internal chamber volume is 131 L. When closed, the air inside the chamber is mixed by a 2.1 W electric fan (air flow 0.7 $m^3 \cdot min^{-1}$).

The main sampling loop links the chambers to analytical instruments via manifold substations. Secondary loops connect the manifold substations to the chambers and a further sampling loop connects a Picarro G2201-i cavity ring-down spectroscopy (CRDS) instrument (Picarro, Santa Clara, CA, USA) to the main loop. Air is pumped through the main loop at approximately 10 $L \cdot min^{-1}$ by a diaphragm pump (Charles Austen B100 SE, Charles Austen Pumps Ltd, Byfleet, UK) and through the CRDS sampling loop at approximately 0.025 $L \cdot min^{-1}$ by a smaller diaphragm pump (Picarro A0702) located downstream from the analyser. The main loop is made of a ⅜-inch 316 stainless steel tube (7.5 mm internal diameter [ID]), polished to 0.8 μm RA and cleaned. This was chosen over cheaper plastic tubing both to minimize gas losses over its long length (46 m) and for longevity. The manifold substations are connected to the individual chambers with a ¼-inch 316 stainless steel tube (3.2 mm ID). The length from the substation to each chamber is 3 m. The total volume of air within the sampling loop (main loop plus one secondary loop to a chamber) is 1.9 L (i.e., 1.5% of the chamber head space). With a flow rate of 10 $L \cdot min^{-1}$, the pressure drop across the sampling loop and associated valves is <1 kPa. The CRDS subsample loop is 1/8-inch ID Bev-A-line flexible plastic tubing (Cole-Parmer, St. Neots, UK) and flexible steel tubing, with a total length of 200 cm.

Figure 1b shows the layout of a manifold substation. Each substation serves four lysimeter chambers, linking them to the main sampling loop in a preprogrammed automated sequence. Each substation contains eight three-port ¼-inch ID solenoid valves (SMC Pneumatics VT307-5DZ-02-Q, Mead Engineering Services Ltd, Lancing, UK), powered by a 24-V DC supply and connected by 6-mm outer diameter (OD), 4-mm ID nylon tubing. The control units for the valves were custom built by Sercon Ltd (Crewe, UK) and are housed in the instrument building. The valves are arranged in three rows (as shown in Figure 1b) and are activated in pairs. The top row determines which of the six substations is connected to the main loop; the other two determine which of the lysimeters in the selected substation is connected.

2.2.2 | Sampling process and protocol for isotope measurements

The opening and closing of the chamber lids and the switching of valves in the sample loops are controlled by software written in Python. The sequence of samplings is randomized across the 24 chambers in each measurement cycle, with three measurement cycles per 24 hr. There are four stages to the process of a chamber measurement, as follows.

1. The lid of the previous chamber is opened and simultaneously the valves connecting it to the sampling loop are deactivated and those connecting the new chamber are activated. Air is pumped continuously through the loop; hence, the gas lines are flushed with air from the external atmosphere (approx. 2.5 min).
2. The lid of the new chamber closes (approx. 0.5 min).
3. Time is allowed for the air in the closed chamber and gas lines to equilibrate, and for the accumulation of CO_2 in the chamber to become linear (approx. 3.5 min).
4. Measurements of the CO_2 concentration and its $\delta^{13}C$ every 0.5 s are continued for a further 13 min.

There is hence a period of 6.5 min from the previous chamber closing to the start of the flux measurements in the new chamber, which lasts 13 min. Therefore, each sampling event takes 19.5 min and so it is possible to sample each of the 24 lysimeters three times over 24 hr.

A three-point slope and offset calibration is performed every 2 months and applied to baseline data collected within 1 month of the calibration date following the manufacturer's guidelines for the Picarro G2201-i analyser. We used three reference standards with differing CO_2 concentrations in air and three with differing $\delta^{13}C$ values spanning the expected range of measured values: (a) 358 μmol·mol^{-1}, −9.35 ‰ (Air Products, Walton-on-Thames, UK), (b) 712 μmol·mol^{-1}, used only

for CO_2 concentration calibration (BOC, UK), (c) 1,010 $\mu mol \cdot mol^{-1}$, −34.44 ‰ (BOC, Guildford, UK), and (d) 800–1,000 $\mu mol \cdot mol^{-1}$, −21.7 ‰ (prepared by mixing 50,000 $\mu mol \cdot mol^{-1}$ from CK Isotopes Ltd, Desford, UK, with CO_2-free (< 1 $\mu mol \cdot mol^{-1}$) air from BOC, UK; used only for $\delta^{13}C$ calibration). Each standard was sampled by flushing it for 4 min through pre-evacuated 12 mL Exetainers® (Labco, Lampeter, UK) with 10 replicates, and CO_2 concentrations and $\delta^{13}C$ values measured at the James Hutton Institute using infra-red gas analysis (EGM4, PP Systems, Amesbury, USA) and isotope-ratio mass spectrometry (IRMS; Finnigan DeltaPlus Advantage connected to a GasBench II System; Thermo Fisher Scientific, Bremen, Germany).

To account for instrumental drift between the three-point slope and offset calibration points, an additional offset calibration is performed thrice daily. Each 24-hr period is divided into three 7.8-hr cycles of measurements, during which each lysimeter is sampled once; between each measurement cycle, the CRDS analyser samples a reference cylinder of compressed air (independently certified CO_2 concentration of 358 $\mu mol \cdot mol^{-1}$ and $\delta^{13}C$ −9.35 ‰) for 12 min 24 s. This gives an 8-min period of stable reference cylinder measurements. The mean CO_2 concentration and $\delta^{13}C$ of this period were compared with the post-calibration values from the same reference cylinder at the proximate three-point slope and offset calibration point. A smoother was generated using a sequence of these reference standard comparisons with a generalized additive model (c.f. Snell et al., 2014), and applied to CO_2 and $\delta^{13}C$ measurements following the three-point slope and offset calibration.

2.2.3 | Flux calculation

For each chamber sampling event, the chamber headspace CO_2 concentration (C) and $\delta^{13}C$ are recorded at approximately 0.5-s intervals (i.e., 1,600 measurements per flux chamber closure) and the results are used to calculate the net CO_2 flux and its overall $\delta^{13}C$ using Keeling plots as follows.

As CO_2 respired by plants and soil microbes mixes with the original CO_2 in a chamber, the $\delta^{13}C$ of the chamber air will change as some function of the isotope composition of the respired CO_2. For steady-state conditions, the $\delta^{13}C$ value will vary in inverse proportion to the CO_2 concentration. From mass balance we have:

$$C = C_0 + C_R, \qquad (1)$$

and

$$\delta^{13}C \times C = \delta^{13}C_0 \times C_0 + \delta^{13}C_R \times C_R, \qquad (2)$$

where subscripts 0 and R refer to the contributions of the initial background and the CO_2 source, respectively. Rearranging Equation (2) and substituting for C_R from Equation (1) gives:

$$\delta^{13}C = \frac{C_0}{C}\left(\delta^{13}C_0 - \delta^{13}C_R\right) + \delta^{13}C_R. \qquad (3)$$

Hence, plots of $\delta^{13}C$ against $1/C$ will have slope $C_0(\delta^{13}C_0 - \delta^{13}C_R)$ and y-axis intercept $\delta^{13}C_R$, which can thus be found. Values of $\delta^{13}C_R$ for individual chamber sampling events were obtained by least squares regression using R (R Core Team, 2017).

The proportions of C_R attributable to soil respiration (C3 origin) and plant respiration (C4), f_{SOM} and f_{plant} respectively, are calculated from:

$$f_{SOM} = \frac{\delta^{13}C_R - \delta^{13}C_{plant}}{\delta^{13}C_{SOM} - \delta^{13}C_{plant}}, \qquad (4)$$

and

$$f_{plant} = 1 - f_{SOM}. \qquad (5)$$

It should be noted that f_{plant} includes all respiration of C substrates of C4 origin, thus combining microbial breakdown of fresh plant inputs in the soil as well as plant respiration.

The SOM and plant end-member $\delta^{13}C$ values were measured as follows. For $\delta^{13}C_{SOM}$, unplanted soil, unexposed to the C4 grass, was moistened to field capacity and packed to a depth of 3 cm in 15-cm internal diameter plastic pipes with acrylic disks glued to their bases. A pneumatically operated gas flux chamber (eosAC, Eosense, Dartmouth, Nova Scotia, Canada) was fitted on top and connected to a Picarro G2201-i isotope analyser and Picarro A0702 diaphragm pump. Measurements of CO_2 respired and its $\delta^{13}C$ were taken and $\delta^{13}C_{SOM}$ obtained using Keeling plots. This gave $\delta^{13}C_{SOM}$ for the Temple Balsall soil = −30.9 ± 0.1‰ (mean ± standard error of seven repeat measurements in two replicate mesocosms). For $\delta^{13}C_{plant}$, seeds of *B. dactyloides* were germinated and grown for 2 months in moist sand heat-treated to remove any organic matter. Mesocosms of grass were placed in gas flux chambers and measurements of CO_2 respired and its $\delta^{13}C$ were taken as above for $\delta^{13}C_{SOM}$. This gave $\delta^{13}C_{plant}$ = −15.3 ± 0.2‰ (mean ± standard error of four repeated measurements of three replicate mesocosms).

2.3 | Tests of the system

2.3.1 | Sampling loop leakiness

The gas permeability of the sampling loop was assessed by bridging the inflow and outflow ports of a lysimeter gas flux chamber with a 1.5-m length of 1/8-inch ID Bev-A-line tubing, via a 4.5-L glass mixing chamber containing a flexible 5 V fan (Aerb Portable USB Powered Cooling Fan, Aerb, Mongkok KL, Hong Kong, China). Expected low and high extremes of CO_2 concentration were tested: 134 ± 7 µmol·mol^{-1} achieved by partially flushing the loop with helium, and $1,526 \pm 29$ µmol·mol^{-1} achieved by injecting a pulse of pure CO_2 into the sampling loop. After 10 min to allow mixing, the CO_2 concentration was monitored over 40 min. The mean concentration was obtained from the values at 1 and 40 min, and the change in concentration was obtained from the difference between these values.

2.3.2 | Measurement response time

The time lag between a CO_2 increase in a lysimeter and its detection by the CRDS analyser was assessed by bridging the lysimeter inflow and outflow ports as above, and injecting 10 mL of 99.8% pure CO_2 (BOC) into a port downstream of the mixing chamber, which took 10 s. The CO_2 concentration was measured over the subsequent 150 s. This was repeated for six lysimeters, one from each manifold substation.

2.3.3 | Precision of CRDS measurements

The precision and instrumental drift of the CRDS measurements were measured by sampling a reference gas cylinder of medical-grade compressed air with 352 µmol·CO_2·mol^{-1} (BOC) for 48 hr and monitoring the absolute CO_2 concentrations and $\delta^{13}C$ values, and their drift over time. This was used to inform the calibration regime detailed previously.

2.3.4 | Concentration dependence of $\delta^{13}C$ measurements

To assess the effect of CO_2 concentration on $\delta^{13}C$ values over the relevant concentration range, gas from a cylinder of pure CO_2 (BOC) was mixed with CO_2-free air (BOC) in 3-L Tedlar® bags (Merck KGaA, Darmstadt, Germany) to give 11 CO_2 concentrations ranging from 80

to 2010 µmol·mol^{-1}. Gas from each Tedlar® bag was pumped at approximately 25 mL·min^{-1} through the CRDS analyser with the exhaust vented to the atmosphere. Starting after 5 min, CO_2 concentrations and $\delta^{13}C$ values were recorded for three periods of 10 min with 3 min between each measurement interval. Each mix was sampled five times in 12-mL Exetainers® (Labco) and the $\delta^{13}C$ of the CO_2 in these was analysed with an IRMS (Finnigan DeltaPlus Advantage connected to a GasBench II System; Thermo Fisher Scientific) at the James Hutton Institute, with four separate measurements per sample. The CRDS and IRMS results were compared to assess the concentration dependence of the CRDS $\delta^{13}C$ measurements.

2.3.5 | Precision of flux measurements

To assess the precision of the CO_2 flux measurements, we generated linear models of CO_2 concentration against time, and $\delta^{13}C$ against $1/C$, for all measurements taken with blackout covers between July 4 and 30, 2018. From these we found the standard errors for the slope of CO_2 concentration against time, and for the intercept of $\delta^{13}C$ against $1/C$ plots. Coefficients of variation were calculated for the flux magnitude and its $\delta^{13}C$ value by finding (a) the standard error of the slope as a percentage of the slope for the CO_2 concentration against time model, and (b) the standard error of the $\delta^{13}C$ against $1/C$ intercept as a percentage of the intercept. Standard errors were used rather than standard deviations in order to find the coefficients of variance of the slope and intercept specifically, rather than of the individual CO_2 concentration and $\delta^{13}C$ measurements used to construct these models. For comparison, inter-lysimeter coefficients of variation were calculated for the same period from the mean CO_2 flux magnitude and its $\delta^{13}C$ for each of 12 lysimeters by finding the standard deviation of this set of means as a percentage of the mean of the 12 lysimeter means.

2.3.6 | Data analysis

Data analysis was conducted using R version 3.5.1. Allan deviation was calculated using the allanvar package in R (R Core Team, 2017). This is an estimate of the frequency stability in an oscillator due to noise rather than systematic errors. It indicates the agreement with the expected relationship between the standard deviation of frequency fluctuations and the infinite-time average of the standard deviation.

3 | RESULTS

3.1 | Growth of the C4 grass

The initial germination and growth of *B. dactyloides* were slow but a healthy and uniform sward was established by June 2018. Peak aboveground growth rates (July 2019) were 4.3 ± 1.3 g·m^{-2}·day^{-1} (mean $\pm$ standard error), as measured from the dry mass of clippings taken from 3 weeks of growth. The active growing season lasted from May to October, which is sufficient to observe seasonal dynamics in plant and soil C fluxes and their response to varied environmental conditions.

3.2 | System performance

3.2.1 | Sampling loop leakiness

Rates of change in concentration due to gas leaks ranged from an increase of 0.31 ± 0.04 μmol·mol^{-1}·min^{-1} at CO_2 concentration $= 134 \pm 3$ μmol·mol^{-1}, to a decrease of 0.28 ± 0.04 μmol·mol^{-1}·min^{-1} at CO_2 concentration $= 1,526 \pm 12$ μmol·mol^{-1} (means $\pm$ standard errors). The volume of the mixing chamber and connected sampling loop was 6.5 L, which is <5% of the volume of a lysimeter chamber and sampling loop. Extremes of headspace CO_2 accumulations measured over 13 min ranged from 25 μmol·mol^{-1} in January to 1,000 μmol·mol^{-1} in July. As such, during a 13-min sampling event, we expect losses of <1% of the total CO_2 increase in January, and a much smaller proportion when fluxes are higher. Given that during the active growing season, losses are an order of magnitude smaller as a proportion of total flux, these leak rates are insubstantial and so we conclude the system as a whole is effectively gas tight.

3.2.2 | Measurement response time

An example time course of CO_2 concentration in a chamber following injection of a CO_2 pulse is shown in Figure 2. The time between injection and CO_2 concentration peaking was 63.4 ± 2.5 s (mean $\pm$ standard error). The mean peak duration was 109.5 ± 5.2 s, although the majority of the peak is contained within 50 s. It is essential that measurements from subsequent lysimeters do not overlap. This test indicated that the mean time requirement for the sampling loop to clear between measurements is 173 s. This demonstrates that the minimum time required between consecutive flux chamber samplings is small using a system such as this, enabling frequent measurements.
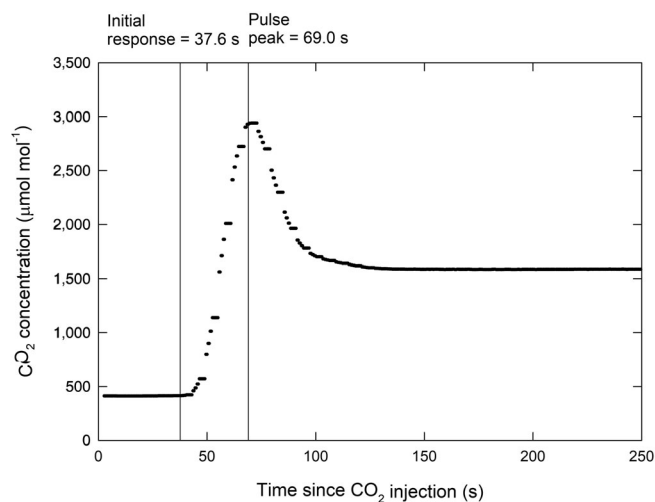

FIGURE 2 Time course of CO_2 concentration in the main sampling loop of the field laboratory following injection of a pulse of pure CO_2 into a mixing chamber downstream from the measurement unit

3.2.3 | CRDS precision and drift

Allan deviation plots for CO_2 concentration and $\delta^{13}C$ were used to assess the role of instrumental noise and drift in measurement precision (Figure 3). These show the standard deviation of measurements taken over a range of time intervals. For both C and $\delta^{13}C$, instrumental noise and drift have antagonistic effects on the precision of measurements. The precision of C measurements improves with increasing measurement time up to a duration of 1,000 s, as increased measurement duration reduced the impact of instrumental noise. At longer durations, however, instrumental drift over the measuring period exceeded the reduction in instrumental noise and the standard deviation of measurements increased with increasing duration. It was therefore necessary to correct for this. The effect of drift was less pronounced for $\delta^{13}C$ measurements and the critical point for this was between 1,000 and 10,000 s.

Using the Allan deviation shown in Figure 3, we assessed the duration and frequency of reference gas measurements required to reduce instrumental imprecision to <0.05 μmol·mol^{-1} for CO_2 concentration and < 0.1 ‰ for $\delta^{13}C$. The required measurement time was 200 s with a frequency of once per 17 hr. This is not a major issue in terms of duration or frequency.

3.2.4 | Concentration dependence of $\delta^{13}C$ measurements

Our assessment of the concentration dependence of $\delta^{13}C$ values, made by diluting a high concentration of CO_2 in air with CO_2-free air, gave less negative $\delta^{13}C$ values by <0.5 ‰
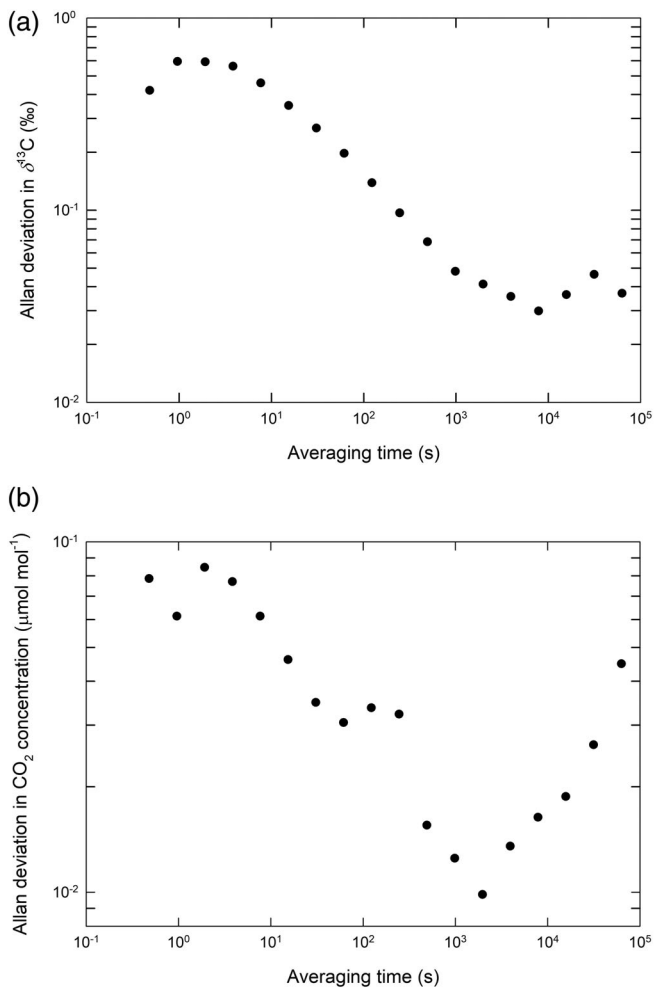
(a)

(b)

FIGURE 3 Allan deviation plots for (a) $\delta^{13}C$ and (b) CO_2 concentration against averaging time. Allan deviation is a measure of the stability to instrumental noise and drift based on measurement frequency: The full measurement period is divided into consecutive clusters of measurements of consistent duration (the "averaging time"), and a measure of the mean variation between cluster averages is calculated (Allan, 1966). This is performed over a range of averaging times to show the antagonistic effects of instrumental noise and drift on the precision of averaged measurements

FIGURE 4 The CO_2 concentration dependence of $\delta^{13}C$ measurements by cavity ring-down spectroscopy (CRDS) compared with isotope-ratio mass spectrometry (IRMS) for gas mixtures made by diluting a high concentration of CO_2 in air with CO_2-free air. Data are means $\pm$ standard error ($n = 3$ for CRDS data, 5 for IRMS data). Line is $\delta^{13}C = -35.5 + 595.0/C$ ($r^2 = 0.99$) fitted to the CRDS data. The two IRMS data points at CO_2 concentrations <250 $\mu mol \cdot mol^{-1}$ were outside the certified limits of detection and are not shown. Standard errors of CO_2 concentrations are less than the widths of the data points

3.2.5 | Accuracy and precision of net CO_2 flux and $\delta^{13}C$ measurements

Figure 5 shows an example plot of CO_2 accumulation in a chamber over time and the corresponding Keeling plot. Some nonlinearity in CO_2 accumulation over time is inevitable because CO_2 accumulation in the chamber will mean the diffusive gradient through the soil to the chamber gradually changes and with it the diffusive flux from the soil will change. To determine the interval over which CO_2 accumulation was effectively linear, we plotted residuals against fitted values for a linear model of CO_2 concentration against time (Supporting Information in Appendix S1). We found a strong deviation of residuals from fitted values over the first 3 min after the chamber lids were closed. With this period excluded, there was some deviation from linearity over the following 13 min, but the deviations in residuals were <1% of the measured CO_2 concentration. This shows CO_2 accumulation was effectively linear over this period and free from perturbations. We plotted residuals against fitted values for a linear model of $\delta^{13}C$ against $1/C$ (Supporting Information in Appendix S1). Although individual residuals were up to 15% of measured $\delta^{13}C$ values, due to instrumental noise, no clear trend was evident to suggest deviation from linearity.

We estimate the precision of the CO_2 flux and flux partitioning measurements from the mean coefficients of variation for respiration measurements in July 2018 to be

as the CO_2 concentration decreased from 2,000 to 400 $\mu mol \cdot mol^{-1}$ (Figure 4). Given that this is in the opposite direction to and far smaller than the trend expected for CRDS instrumental bias (Becker et al., 2012; Snell et al., 2014), and the trend is similar for measurements by IRMS (Figure 4), we attribute it to small differences in contamination with laboratory air during the sampling process. From the line fitted to the CRDS data in Figure 4, the CO_2 concentration corresponding to the $\delta^{13}C$ value typical of laboratory air (≈ -8 ‰) is 22 $\mu mol \cdot mol^{-1}$, which is consistent with small, inevitable contamination of the Tedlar bags in the process of measurements. The scatter in the data is greater for the IRMS measurements, presumably because of differences in the sampling process to that for the CRDS (Section 2.3.4).
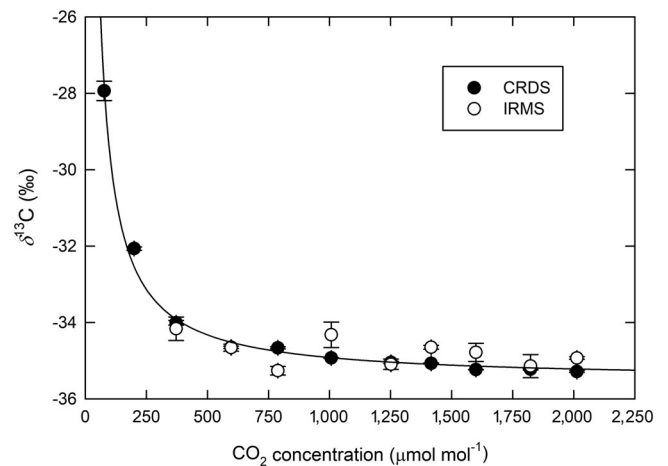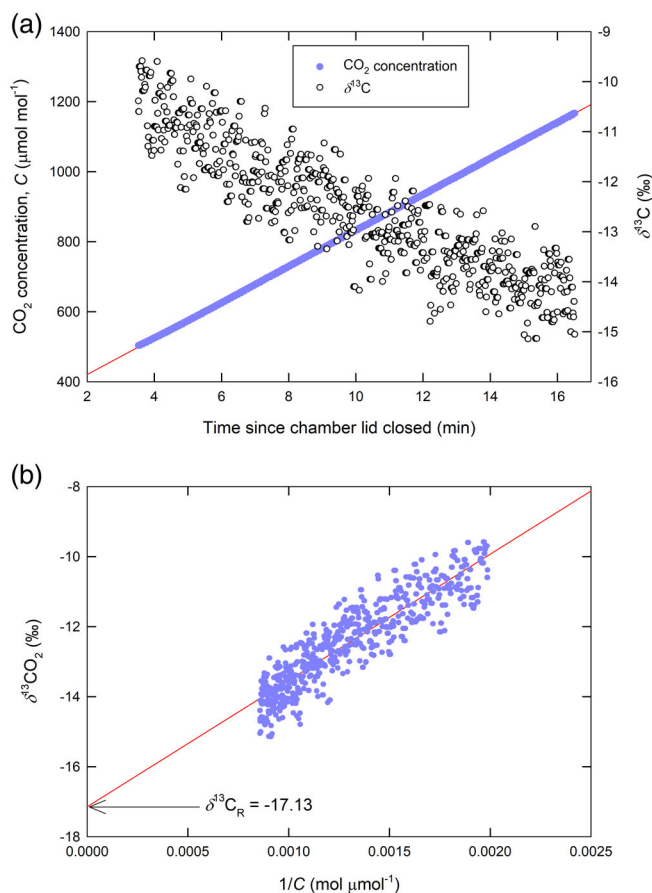
FIGURE 5 Example of (a) CO_2 accumulation and changes in $\delta^{13}C$ in a lysimeter chamber beginning 3.5 min after closing the lid, and (b) the corresponding Keeling plot. Data are individual measurements; lines are linear regressions with fitted parameters (± standard errors): $C = (317.9 \pm 0.1) + (51.39 \pm 0.01)t$, $r^2 = 1.00$; $\delta^{13}C = (3,606 \pm 41)/C - (17.14 \pm 0.05)$, $r^2 = 0.81$. The $\delta^{13}C$ of plant and soil respiration ($\delta^{13}C_R$ in Equation 3) is inferred from the value at $1/C = 0$

±0.04% for the flux and ±0.04% for the flux partitioning. These are substantially smaller than the corresponding coefficients of variation between lysimeters over the same period (±6.56% and ±3.27%, respectively).

3.3 | Illustrative diurnal and seasonal patterns

Figure 6 shows clear diurnal patterns in both plant and soil respiration, and variation over the growing season. Plant and soil C fluxes in October, near the end of the grass's growing season, were approximately a third of those in July, and the diurnal variations were correspondingly reduced.

Figure 7 shows soil temperature and moisture measurements taken over the same period as in Figure 6a. The diurnal variation in soil temperature at 120-mm
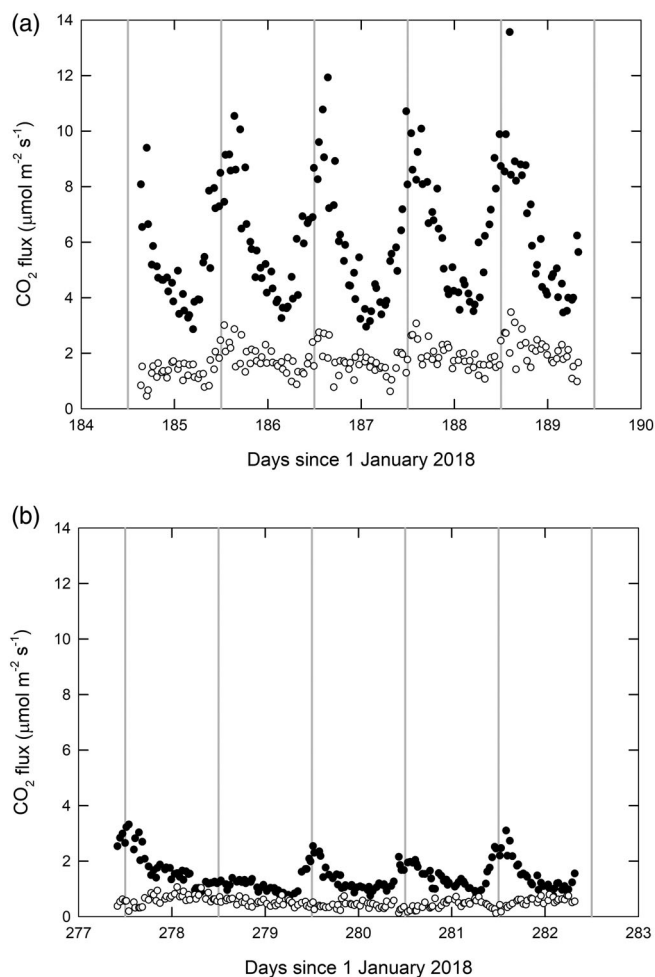

FIGURE 6 Plant (closed symbols) and soil (open symbols) respiration fluxes for (a) July 4–9 and (b) October 5–10, 2018. Data are pooled measurements from 12 lysimeters each measured thrice daily; individual points are for a single lysimeter. Grey lines indicate midday

depth, and at 60-mm depth (data not shown), matched the variation in plant C flux. A diurnal pattern is also evident for soil moisture, with faster drying during the day than at night, with the changes between days punctuated by watering or rainfall events. There were also seasonal trends, with an overall increase in soil moisture later in the season (data not shown).

4 | DISCUSSION

4.1 | Performance of the measurement system

We have shown that the five potential sources of error investigated do not significantly affect the measured CO_2 fluxes or their isotope signatures. These sources of error are gas leaks from the sampling loops, the response time
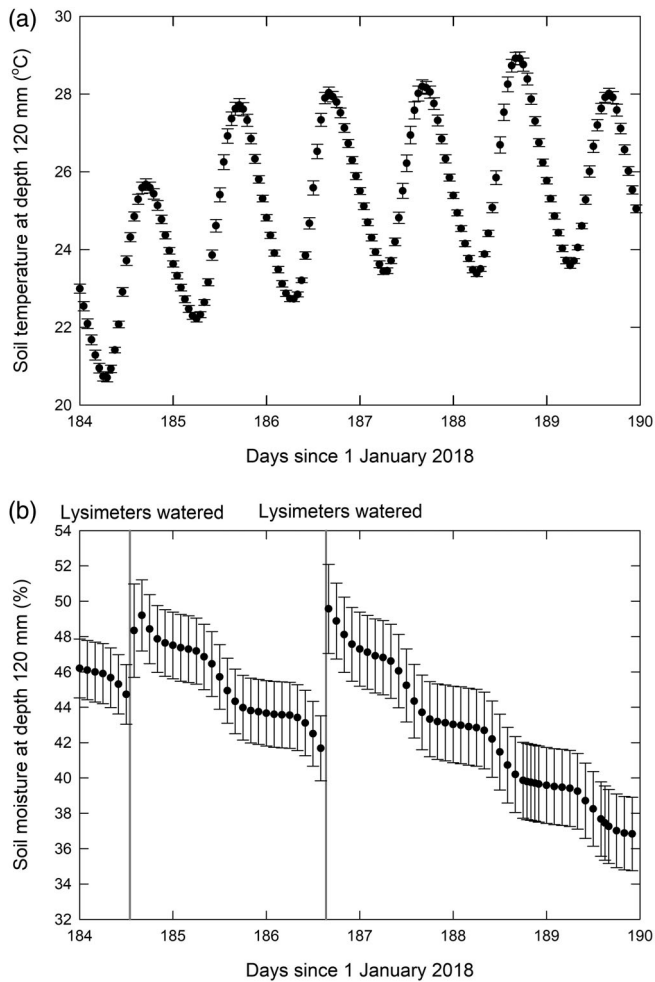
FIGURE 7 Diurnal patterns of (a) soil temperature and (b) volumetric soil moisture content. Data are means ± standard errors of measurements from 12 lysimeters at 120-mm depth. For clarity, one measurement per hour is shown in (a) and two in (b)

of the measurement system, the instrument precision after correcting for drift, the concentration dependence of isotope measurements, and the linearity of CO_2 accumulation in the chambers. These potential sources of error depend on the engineering quality of the system and instruments, not on the particular plant–soil system tested.

After correcting for noise and drift, the precision of our $\delta^{13}C$ measurements by CRDS was <0.1‰. This is two orders of magnitude smaller than the difference in $\delta^{13}C$ between typical C4 plant and C3 soil end-members, so is adequate for our purposes. Our $\delta^{13}C$ measurements were effectively independent of CO_2 concentration over the relevant range, given the large $\delta^{13}C$ differences we need to measure. Snell et al. (2014) found $\delta^{13}C$ values measured by an earlier Picarro CRDS instrument (G1101-*i*) increased nonlinearly with increasing CO_2 concentration, as compared with those measured by an isotope ratio mass spectrometer. Evidently this bias has been satisfactorily corrected in the newer Picarro G2201-*i* instrument

used in this study. We note there is the possibility of spectral interferences from matrix gases (H_2O, O_2) in isotope assays by laser spectroscopy, as discussed by Rella, Hoffnagle, He, and Tajima (2015) for CH_4 and Harris et al. (2020) for N_2O. It is therefore important to minimise differences in composition between samples and reference gases.

The Keeling plot method of calculating the flux $\delta^{13}C$ requires a linear relationship between $\delta^{13}C$ and $1/C$. To the extent that CO_2 accumulation in the chamber alters the concentration gradient through the soil, diffusion is no longer at steady state and so $\delta^{13}C$ values will be biased because of the slower diffusion of $^{13}CO_2$ than $^{12}CO_2$ (Moyes, Gaines, Siegwolf, & Bowling, 2010; Nickerson & Risk, 2009; Ohlsson, 2010). We tested for this by plotting residuals against fitted values for a linear model of $\delta^{13}C$ against $1/C$ (Supplementary Material). Very little nonlinearity was evident, and slopes of lines of best fit for residuals were close to zero. This indicates there was no substantial isotopic bias over the course of a 13-min chamber measurement.

To allow an additional complete set of flux measurements from the 24 lysimeters in a day would require the measurement time to be reduced from 13 to 8 min. This increases the mean coefficients of variance to ±0.05% for the flux and ±0.77% for the flux partitioning. This remains a low level of imprecision and would be acceptable to allow greater temporal resolution of measurements.

Advantages of a fully automated system over manual systems include the much finer temporal resolution that can be achieved. We are able to measure and partition fluxes from each lysimeter at least four times per day, which is sufficient to resolve diurnal variations in all 24 lysimeters in one 24-hr period. Automation also allows semi-continuous measurements over a full season and beyond. That is not practicable with manual methods.

The clear diurnal and seasonal patterns in both plant and soil respiration show that the system is sufficiently sensitive to separate these. The system was also capable of resolving diurnal and seasonal variation in soil temperature and moisture. The diurnal temperature variation was more marked than that in moisture, presumably due to faster heat than moisture transfer through soil. The variation in moisture between lysimeters is much larger than that for temperature, presumably due to greater sensitivity of moisture to plant and soil heterogeneity.

4.2 | Separation of plant and soil C fluxes

Most previous systems for separating plant and soil C fluxes seek to isolate the belowground plant and soil fluxes from the aboveground plant fluxes, whereas, by

enclosing the aboveground plant parts as well as the soil surface in our flux chambers, we measure whole-plant and soil fluxes. This allows us to measure both C fixation by the plants in photosynthesis when the chambers are left transparent and the respiration-only flux when the chambers are blacked out. Hence, coupled with measurements of leaching losses from the base of the lysimeters, we can obtain a complete C balance for the plant–soil system.

Resolution of the measured net flux into plant and soil components requires values of the plant and soil end-member $\delta^{13}C$ values in Equation (4). Because we measure whole-plant respiration, the relevant plant end-member is that for the whole plant. Also, because we measure the whole flux, the flux is more dominated by plant respiration than in belowground only systems, and the flux partitioning is correspondingly more sensitive to errors in the plant $\delta^{13}C$ end-member. What potential errors are specific to our system?

We measure the plant $\delta^{13}C$ end-member with plants grown in C-free sand using opaque chambers. It is known that CO_2 respired by darkened, light-adapted leaves is enriched in ^{13}C during the first minutes following darkening due to rapid changes in leaf biochemistry (Barbour et al., 2011). Because our plant end-member is measured under similar conditions to the respiration measurements in the lysimeters, with opaque chambers closed for a similar period, this should be a small source of error.

Some proportion of the belowground respiration may escape from the soil via the roots to the plant shoots and atmosphere, and this additional soil flux will be captured by our system. It is a large part of the net flux in wetland plants with aerenchymatous roots such as rice (Kirk et al., 2019), but also a significant part of the flux in some dryland plants via the xylem stream (Aubrey & Teskey, 2009). Assuming that this CO_2 has the same $\delta^{13}C$ as soil respiration (i.e., it undergoes no isotopic fractionation during its passage through the plant), the flux will be correctly accounted for in the total soil flux. That this additional flux is captured by our system, but not by systems in which only the belowground flux is measured, is an advantage.

The $\delta^{13}C$ of root respiration may be 2–3‰ more negative than that of shoot respiration (Bowling et al., 2008). This may introduce error to the extent that root:shoot ratios and plant physiological status differ between the lysimeters and the end-member measurement system. However, all other approaches using plant end-member measurements are subject to similar constraints.

Other generic sources of error in the plant end-member $\delta^{13}C$, shared with other systems, include the effects of varying plant nutrient status, lighting, temperature, moisture and mycorrhizal colonization (Bowling et al., 2008; Paterson et al., 2009). Generic sources of error in the soil end-member $\delta^{13}C$ shared with other systems include that the soil end-member is generally measured in disturbed, repacked soil, but soil disturbance exposes labile ^{13}C-depleted substrates that decompose more rapidly than average SOM (Zakharova et al., 2014).

4.3 | Movement of the C4 signal through the soil

The switch from C3 to C4 vegetation means that the plant C is homogenously labelled, unlike more widely used pulse labelling to partition plant and soil C sources, so that the isotopic signature of C entering the soil is constant, allowing a quantitative partitioning of the CO_2 efflux. Over time, the C4 signal from the decomposing plant residues will move through soil carbon pools with differing turnover rates and alter their $\delta^{13}C$ signatures. In principle, this provides a means of testing soil carbon models and measuring the rates of turnover of model SOM pools. This requires that the pools and their $\delta^{13}C$ signatures are measurable and that the movement of the C4 signal through the pools is not too rapid. An indicative calculation of the rate of movement is as follows.

Assuming a simple one-pool model of SOM turnover, the ratio of the ^{13}C content of the soil at time t after switching to C4 grass to that at steady state is $C_t^*/C_\infty^* = 1 - e^{-kt}$, where k is the decomposition rate constant (definitions of variables are given in the Supporting Information in Appendix S1). A typical value of k for grassland soils in England and Wales is 0.04 years (Kirk & Bellamy, 2010). This gives $C_t^*/C_\infty^* = 0.04$ at $t = 1$ year. That is, following a switch from C3 to C4 grass, the soil ^{13}C content would change by only 4% towards that of the C4 grass over a year.

This calculation lumps together all the SOM in a single pool with a single rate constant, whereas in reality there is a continuum of SOM forms and accessibilities turning over at different rates, and in the early stages a larger proportion of the C4-C will be in more rapidly turned over SOM pools. Rate constants for more labile SOM may be an order of magnitude larger than for the more humified material. Nonetheless, the calculation indicates the order of magnitude of the rate of progress of the C4 signal through the SOM and that the progress through different pools would be detectable over one to many growth seasons.

5 | CONCLUSIONS

1. The automated field system presented measures net ecosystem respiration fluxes and their plant and soil

components with sufficient precision to resolve diurnal and seasonal patterns in both.

2. Errors in CO_2 concentration and isotope measurements due to the measurement system and instruments were negligible relative to the required precision.

3. For the loamy grassland soil and US prairie grass tested, we estimate the precision of measurements to be $\pm 0.04\%$ for CO_2 fluxes and $\pm 0.40\%$ for flux partitioning.

4. By eliminating manual sampling, this system provides a means of gathering long-term near-continuous C flux data under realistic field conditions.

CONFLICT OF INTEREST
The authors have no conflicts of interest related to the work presented in this manuscript.

AUTHOR CONTRIBUTIONS
G.K. conceived and coordinated the construction of the field laboratory. C.M., G.K., W.O. and E.P. conceived this study. C.M. carried out the experimental work and data analysis. BI wrote the software for the lysimeter sampling process. C.M. and G.K. wrote the initial manuscript and all contributed to the final version.

DATA AVAILABILITY STATEMENT
The data used in this article will be available at CORD c/o the Cranfield University Library.

ORCID
Christopher S. McCloskey https://orcid.org/0000-0002-4439-8263
Wilfred Otten https://orcid.org/0000-0002-3847-9825
Eric Paterson https://orcid.org/0000-0003-1512-7787
Ben Ingram https://orcid.org/0000-0003-4557-4342
Guy J. D. Kirk https://orcid.org/0000-0002-7739-9772

REFERENCES
Allan, D. W. (1966). Statistics of atomic frequency standards. *Proceedings of the IEEE*, *54*, 221–230.

Aubrey, D. P., & Teskey, R. O. (2009). Root-derived CO_2 efflux via xylem stream rivals soil CO_2 efflux. *New Phytologist*, *184*, 35–40.

Bader, N. E., & Cheng, W. (2007). Rhizosphere priming effect of *Populus fremontii* obscures the temperature sensitivity of soil organic carbon respiration. *Soil Biology & Biogeochemistry*, *39*, 300–306.

Balesdent, J., Mariotti, A., & Guillet, B. (1987). Natural ^{13}C abundance as a tracer for studies of soil organic matter dynamics. *Soil Biology and Biochemistry*, *19*, 25–30.

Barbour, M. M., Hunt, J. E., Kodama, N., Laubach, J., McSeveny, T. M., Rogers, G. N. D., ... Wingate, L. (2011). Rapid changes in $\delta^{13}C$ of ecosystem-respired CO_2 after sunset are consistent with transient ^{13}C enrichment of leaf respired CO_2. *New Phytologist*, *190*, 990–1002.

Becker, M., Andersen, N., Fiedler, B., Fietzek, P., Körtzinger, A., Steinhoff, T., & Friedrich, G. (2012). Using cavity ringdown spectroscopy for continuous monitoring of $\delta^{13}C(CO_2)$ and fCO_2 in the surface ocean. *Limnology and Oceanography: Methods*, *10*, 752–766.

Bowling, D. R., Pataki, D. E., & Randerson, J. T. (2008). Carbon isotopes in terrestrial ecosystem pools and CO_2 fluxes. *New Phytologist*, *178*, 24–40.

Carney, K. M., Hungate, B. A., Drake, B. G., & Megonigal, J. P. (2007). Altered soil microbial community at elevated CO_2 leads to loss of soil carbon. *Proceedings of the National Academy of Sciences USA*, *104*, 4990–4995.

Dijkstra, F. A., & Cheng, W. (2007). Interactions between soil and tree roots accelerate long-term soil carbon decomposition. *Ecology Letters*, *10*, 1046–1053.

Farquhar, G. D., Ehleringer, J. R., & Hubick, K. T. (1989). Carbon isotope discrimination and photosynthesis. *Annual Review of Plant Physiology and Plant Molecular Biology*, *40*, 503–537.

Garcia-Pausas, J., & Paterson, E. (2011). Microbial community abundance and structure are determinants of soil organic matter mineralisation in the presence of labile carbon. *Soil Biology and Biochemistry*, *43*, 1705–1715.

Harris, S. J., Liisberg, J., Xia, L., Wei, J., Zeyer, K., Yu, L., ... Mohn, J. (2020). N_2O isotopocule measurements using laser spectroscopy: analyzer characterization and intercomparison. *Atmospheric Measurement Techniques Discussions*, *13*(5), 2797–2831. https://doi.org/10.5194/amt-2019-451

Iversen, C. M., Keller, J. K., Garten, C. T., Jr., & Norby, R. J. (2012). Soil carbon and nitrogen cycling and storage throughout the soil profile in a sweetgum plantation after 11 years of CO_2-enrichment. *Global Change Biology*, *18*, 1684–1697.

Kirk, G. J. D., & Bellamy, P. H. (2010). Analysis of changes in organic carbon in mineral soils across England and Wales using a simple single-pool model. *European Journal of Soil Science*, *61*, 406–411.

Kirk, G. J. D., Boghi, A., Affholder, M. C., Keyes, S. D., Heppell, J., & Roose, T. (2019). Soil carbon dioxide venting through rice roots. *Plant Cell and Environment*, *42*, 3197–3320.

Lu, J., Dijkstra, F. A., Wang, P., & Cheng, W. (2009). Roots of non-woody perennials accelerated long-term soil organic matter decomposition through biological and physical mechanisms. *Soil Biology and Biochemistry*, *134*, 42–53.

Millard, P., Midwood, A. J., Hunt, J. E., Whitehead, D., & Boutton, T. W. (2008). Partitioning soil surface CO_2 efflux into autotrophic and heterotrophic components using natural gradients in soil $d^{13}C$ in an undisturbed savannah soil. *Soil Biology and Biochemistry*, *40*, 1575–1582.

Moinet, G. Y. K., Midwood, A. J., Hunt, J. E., Whitehead, D., Hannam, K. D., Jenkins, M., ... Millar, P. (2018). Estimates of rhizosphere priming effects are affected by soil disturbance. *Geoderma*, *313*, 1–6.

Moyes, A. B., Gaines, S. J., Siegwolf, R. T. W., & Bowling, D. R. (2010). Diffusive fractionation complicates isotopic partitioning of autotrophic and heterotrophic sources of soil respiration. *Plant Cell and Environment*, *33*, 1804–1819.

Nickerson, N., & Risk, D. (2009). Keeling plots are non-linear in non-steady state diffusive environments. *Geophysical Research Letters*, *36*, L08401.

Ohlsson, K. E. A. (2010). Reduction of bias in static closed chamber measurement of $\delta^{13}C$ in soil CO_2 efflux. *Rapid Communications in Mass Spectrometry*, *24*, 180–184.

Paterson, E., Midwood, A. J., & Millard, P. (2009). Through the eye of the needle: A review of isotope approaches to quantify microbial processes mediating soil carbon balance. *New Phytologist*, *184*, 19–33.

R Core Team. (2017). *R: A language and environment for statistical computing*. Vienna, Austria: R Foundation for Statistical Computing.

Rella, C. W., Hoffnagle, J., He, Y., & Tajima, S. (2015). Local- and regional-scale measurements of CH_4, $\delta^{13}CH_4$, and C_2H_6 in the Uintah Basin using a mobile stable isotope analyser. *Atmospheric Measurement Techniques*, *8*, 4539–4559.

Schnyder, H., Schäufele, R., Lötscher, M., & Gebbing, T. (2003). Disentangling CO_2 fluxes: Direct measurements of mesocosm-scale natural abundance $^{13}CO_2/^{12}CO_2$ gas exchange, ^{13}C discrimination, and labelling of CO_2 exchange flux components in controlled environments. *Plant Cell and Environment*, *26*, 1863–1874.

Snell, H. S. K., Robinson, D., & Midwood, A. J. (2014). Minimising methodological biases to improve the accuracy of partitioning soil respiration using natural abundance ^{13}C. *Rapid Communications in Mass Spectrometry*, *28*, 2341–2351.

Taneva, L., Pippen, J. S., Schlesinger, W. H., & Gonzàlez-Maler, M. A. (2006). The turnover of carbon pools contributing to soil CO_2 and soil respiration in a temperate forest exposed to elevated CO_2 concentration. *Global Change Biology*, *12*, 983–994.

USDA. (2019). *Bouteloua dactyloides (Nutt.) J.T. Columbus Buffalograss*. Washington, DC: United States Department of Agriculture Retrieved from https://plants.usda.gov/core/profile?symbol=BODA2 (accessed on November 14, 2019).

Zakharova, A., Midwood, A. J., Hunt, J. E., Graham, S. L., Artz, R. R. E., Turnbull, M. H., ... Millard, P. (2014). Loss of labile carbon following soil disturbance determined by measurement of respired $\delta^{13}CO_2$. *Soil Biology & Biochemistry*, *68*, 125–132.

Zhu, Z.-C., Di, D.-R., Ma, M.-G., & Shi, W.-Y. (2019). Stable isotopes in greenhouse gases from soil: A review of theory and application. *Atmosphere*, *10*, 377.

SUPPORTING INFORMATION

Additional supporting information may be found online in the Supporting Information section at the end of this article.